



**HAL**  
open science

# Electrochemical pressure impedance spectroscopy applied to polymer electrolyte membrane fuel cells for investigation of transport phenomena

Anantrao-Vijay Shirsath, Stéphane Raël, Caroline Bonnet, François Lapique

## ► To cite this version:

Anantrao-Vijay Shirsath, Stéphane Raël, Caroline Bonnet, François Lapique. Electrochemical pressure impedance spectroscopy applied to polymer electrolyte membrane fuel cells for investigation of transport phenomena. *Electrochimica Acta*, 2020, 363, pp.137157. 10.1016/j.electacta.2020.137157 . hal-02977172

**HAL Id: hal-02977172**

**<https://hal.univ-lorraine.fr/hal-02977172v1>**

Submitted on 17 Oct 2022

**HAL** is a multi-disciplinary open access archive for the deposit and dissemination of scientific research documents, whether they are published or not. The documents may come from teaching and research institutions in France or abroad, or from public or private research centers.

L'archive ouverte pluridisciplinaire **HAL**, est destinée au dépôt et à la diffusion de documents scientifiques de niveau recherche, publiés ou non, émanant des établissements d'enseignement et de recherche français ou étrangers, des laboratoires publics ou privés.



Distributed under a Creative Commons Attribution - NonCommercial 4.0 International License

## **Electrochemical pressure impedance spectroscopy applied to polymer electrolyte membrane fuel cells for investigation of transport phenomena**

Anantrao Vijay SHIRSATH<sup>1</sup>, Stéphane RAËL<sup>2,1</sup>, Caroline BONNET<sup>1</sup>, François LAPICQUE<sup>1\*</sup>

<sup>1</sup> Laboratory for Reactions and Chemical Engineering, CNRS – University of Lorraine, BP 20451, 54001 Nancy, France

<sup>2</sup> Group of Research in Electrical Engineering of Nancy (GREEN), University of Lorraine, 2 Avenue de la Forêt de Haye, BP 90161, 54505 Vandoeuvre-lès-Nancy, France

### **Abstract**

The performance of proton exchange membrane fuel cells (PEMFC) is partly governed by complex, coupled transport processes at high polarization which usually occur in the low frequency region. Electrochemical impedance spectroscopy (EIS) is a powerful tool to extract valuable information about ohmic, charge and mass transport processes but fails marginally below 1 Hz as limited information on mass transport can be extracted. In this work, electrochemical pressure impedance spectroscopy (EPIS) was performed by applying fluctuations of the gas pressure at the fuel cell cathode outlet in the frequency range 1 mHz – 1 Hz to peek into transport processes. An experimental bench was designed and setup for reliable EPIS measurements on a single 100 cm<sup>2</sup> FC. Conditions of pressure modulation in the test bench were thoroughly examined, leading to a standard protocol of operation. Two cases were studied to better understand and differentiate the various transport phenomena occurring in fuel cell operation. First, EPIS spectra exhibit striking profile differences in both modules and phases, with variations of the oxygen mole fraction in the cathode gas fed, evidencing gas diffusion phenomena. Moreover, sensitivity of impedance modulus and phase to mass transport control by the presence of liquid water could be shown. EPIS has been shown here to become an attractive complementary technique to EIS, but further experimental and theoretical works are required for full beneficitation of this promising tool.

**Keywords:** Electrochemical pressure impedance spectroscopy, Proton exchange membrane fuel cell, transport phenomena, diffusion, water management.

(\*) Correspondence: Dr. Francois Lapicque francois.lapicque@univ-lorraine.fr

## **1. Introduction**

According to the report published by the Intergovernmental Panel on Climate Change in 2018, the increased CO<sub>2</sub> emissions are ultimately responsible for increasing the global temperature by an average of 1.5 °C during the last three decades [1]. Therefore, the demand to shift from fossil fuel-based energy sources to renewable energy sources has been increasing exponentially. One of the promising renewable and clean energy sources is the fuel cell [2,3]. Particularly polymer electrolyte membrane fuel cells (PEMFCs) hold the key to become a power source for numerous applications because of their higher power density, ease of operation, and compact structure [4,5]. PEMFCs are electrochemical devices with simple construction and mode of operation, whose performance and durability are governed by various processes e.g. charge transfer, reactant mass transport, and water transport. These processes are highly coupled and are responsible for losses in performance and durability over time which can be diagnosed and identified using various diagnosis techniques [6,7].

Electrochemical impedance spectroscopy (EIS) is one of the most well-known, nondestructive characterization techniques of electrochemical systems [8]. EIS is based on the analysis of the dynamic relationship between voltage and current. A sine modulation in current or voltage is applied to the system over a frequency range (typically 10 kHz to 100 mHz), and the response of voltage or current is observed. The ratio of voltage over current oscillations forms the complex impedance at the frequency considered. Therefore, EIS applied to fuel cells, provides crucial information about ohmic phenomena at high frequency, charge transfer kinetics in the range 5 Hz to 1 kHz and can indicate to some extent on losses due to transport rates in the lower frequency region [9,10]. As a matter of fact, momentum and mass transports being processes with

characteristic time constants in the order of the second or more, can be observed in the low-frequency region below a few Hz [8–10]. EIS fails marginally in this frequency region since limited information is usually extracted below 1 Hz. In addition, EIS may appear struggling to differentiate between various transport phenomena because of the possible masking of mass transport phenomena by charge transfer phenomena in the catalyst layer with comparable time constants at a fraction of second [8,9].

Based on the principle of EIS, by establishing and studying the dynamic relationship between variables other than electrical ones, one can gain crucial information about slow processes inside the fuel cell. PEMFCs offer gas pressure as such a variable. First, fuel cell performance is enhanced if the cathode side is set at a higher pressure than the anode side [10]. Moreover, increasing back-pressure in a PEMFC has been reported to enhance the fuel cell performance by boosting the fuel cell thermodynamics according to Nernst law, increasing exchange current density, while improving the current distribution due to the higher oxygen concentration at the cathode [11]. Besides, transfer rates of gaseous reactants are improved at higher pressures, with less frequent transient flooding by the liquid water formed. Accordingly, at higher cathode back-pressure, smaller low frequency loops in the Nyquist EIS spectrum express lower mass transport control of performance. However, no precise comments could be made on spatial transport and hydration imbalance in the cathode side due to insufficient accuracy of the data at low frequency [10,12–14].

The first investigation on the dynamic relationship between pressure and voltage conducted by Niroumand et al. [15], showed that oscillations of the cathode back-pressure in polymer electrolyte fuel cells result in cell voltage oscillations with an identical frequency in the range 0.1 - 20 Hz, suggesting the potential of the original technique to better understand transport

processes. Hartmann et al. [16] examined the various dynamic relationships between gas pressure, current, and voltage in electrochemical cells with gaseous reactants, and defined a new type of impedance called electrochemical pressure impedance and its related spectroscopy (EPIS). Application of EPIS to sodium-oxygen batteries by monitoring pressure amplitude of the enclosed oxygen reservoir in relation to electrical variables, yielded vital information about hydration imbalance, changes in reactant distribution and their effects on mass transport. EPIS was shown to be significantly sensitive to oxygen transport properties of porous electrodes. Gröbl et al. [17] established through numerical simulations that EPIS can be used to distinguish between various transport processes e.g. gas diffusion in the porous structures or water transport in the low-frequency regime, in a domain where EIS fails to access [17]. Engebretsen et al. [18] applied EPIS to PEMFC by modulating the cathode outlet pressure between 10 mHz and 100 Hz using a loudspeaker assembly. Despite appreciable noise in the data acquired, they demonstrated the potential of EPIS to investigate transport processes e.g., water transport, diffusive and convective gas transports more accurately than EIS.

The work deals with the design and operation of an experimental bench for reliable investigation of EPIS on a single 100 cm<sup>2</sup> PEM fuel cell installed in a full test bench with air humidification. The sinusoidal modulation in the cathode backpressure applied using a pressure regulator at the cell outlet, induced the sinusoidal harmonic response in voltage. In the frequency range 1 mHz - 1 Hz, care was taken to determine suitable modulation conditions allowing safe fuel cell operation, sufficient amplitude of the voltage signal, but with restricted distortion. Then, EPIS was tested for various operating conditions e.g. oxygen partial pressure and gas humidification.

## **2. Materials and methods**

### **2.1 Experimental bench**

The laboratory test bench has been designed for a 100 cm<sup>2</sup> single PEM fuel cell (UBzM, Germany) and set up. Figure 1 shows the flow diagram of the experimental bench with the various ancillaries and the variables measured. The membrane electrode assembly (MEA) of MEA-H500 model (UBzM, Germany) formed by a Nafion™-212 membrane and catalysts layers loaded with 0.4 mg Pt cm<sup>-2</sup>. The gas diffusion layers (GDL) used were of Sigracet 29 BC grade comprising an MPL and treated with 5% PTFE. A Kikusui™ power unit was used as an external load to vary the current density.

The bench was controlled by dSPACE® real-time electronic card, and the user interface was provided by the Controldesk software. The setup was linked with MATLAB-Simulink 2017® mathematical environment for all control settings such as reference and measured inlet gas flow rates, reference and measured outlet pressure, current density, data acquisition and processing, and emergency shutdown settings.

Hydrogen was always fed dry to the anode of the fuel cell, whereas air was humidified. The experimental bench was also equipped with pure oxygen to be supplied at the cathode instead of air or to be mixed with air (depending upon the planned experiments and operating conditions). The humidifier installed was a double walled 1.85 L vessel partly filled with SS grid packing and de-ionized water. The water level was always kept at 1000 ± 50 mL with a peristaltic pump supplying de-ionized water. Upon circulation of warm water in the double envelope, the relative humidity (RH) was adjusted to the desired level by the compared temperatures in the fuel cell (fixed at 55°C) and in the humidifier.

The gas flow rates were chosen to allow excess in the molar amount of reacting gas. Factor  $\lambda_{H_2}$  was fixed at 1.2 and unless specified,  $\lambda_{O_2}$  was at 2.5. Both gas inlet streams were preheated to 60 °C to prevent cold spot and condensation of water vapor. Inlet and outlet pressures of both cell

compartments were monitored by pressure sensors. The outlet gas streams circulated in double-walled condensers with cooling water at 5 °C, allowing condensation of the major part of the exiting water. This arrangement enabled the water management through mass balances to be followed, and to preserve the outlet pressure regulators which have a low moisture tolerance. Moreover, the regulator for backpressure modulation being a diaphragm-based device did not allow frequencies larger than a few Hz.

## 2.2 Measurement principle

Pressures at both cathode and anode outlets were first fixed at a steady level  $\bar{P}_{out}$ , by means of the pressure controllers installed at each gas stream outlet. Then keeping the anode back-pressure constant at  $\bar{P}_{out}$ , sinusoidal pressure fluctuations at the cathode back-pressure were applied with amplitude  $\Delta P_{out}$  and frequency  $f$ , resulting in fluctuations of the cell voltage to be continuously monitored at constant current density.

The frequency domain considered for the study was 1 mHz to 1 Hz. A set of a definite number of periods of certain frequency was recorded; this set was termed as acquisition. Usually, 10 periods per acquisition were recorded at 10 mHz and above, and only three periods for lower frequencies. The current density levels considered were 0.2, 0.4, 0.8 and 1 A.cm<sup>-2</sup>. The electrochemical pressure impedance is the transfer function describing the response of the fuel cell voltage variations  $\tilde{U}(t)$  to outlet pressure fluctuations  $\tilde{P}_{out}(t)$ . In a general matter, it can be written in Laplace domain as

Equation 1 
$$Z_{U-P}(s) = \frac{\tilde{U}(s)}{\tilde{P}_{out}(s)}$$

where  $s$  is the Laplace variable. In frequency domain ( $s = i\omega$ , with  $\omega$  the angular frequency, and  $i$  the pure imaginary number of modulus 1 and argument  $\pi/2$ ), the electrochemical pressure

impedance can be represented, as commonly for an harmonic impedance, through a modulus and a phase shift :

$$\text{Equation 2} \quad |Z_{U-P}(\mathbf{i}\omega)| = \left| \frac{\tilde{U}(\mathbf{i}\omega)}{\tilde{P}_{out}(\mathbf{i}\omega)} \right|$$

$$\text{Equation 3} \quad \varphi(Z_{U-P}(\mathbf{i}\omega)) = \text{arg}[\tilde{U}(\mathbf{i}\omega)] - \text{arg}[\tilde{P}_{out}(\mathbf{i}\omega)]$$

corresponding in time domain, if  $\tilde{P}_{out}(t)$  is chosen as phase shift reference, by the following definitions:

$$\text{Equation 4} \quad \tilde{P}_{out}(t) = \Delta P_{out} \cdot \sin(\omega t)$$

$$\text{Equation 5} \quad \tilde{U}(t) = |Z_{U-P}(\mathbf{i}\omega)| \cdot \Delta P_{out} \cdot \sin[\omega t + \varphi(Z_{U-P}(\mathbf{i}\omega))]$$

In practice, signals could be distorted, in particular above a few hundred mHz, because of the dynamic limitations of the pressure controller. Consequently, modulus and phase calculations were carried out on signal first harmonics (i.e. on signal  $\omega$ -components), extracted from measured signals by means of Fourier analysis. For this purpose, signal acquisition was performed at a minimum rate of 1000 samples per period. Signals may be blurred by some electrical noise, especially the fuel cell voltage. As previously mentioned, a definite number of periods were recorded for each frequency. In the post-processing procedure, all these periods were used to build averaged one-period signals, which enables to reduce the noise level, thus, to increase accuracy of Fourier analysis.

Preliminary tests were carried out to check satisfactory good operation of the various components of the test bench and to observe the preliminary response of the system to back-pressure modulation. Moreover, these tests were also proved to be useful in determining the constraints in performing EPIS tests on the laboratory test bench, for the sake of reliable, valuable EPIS data.

### 3. Preliminary EPIS measurements: evidence of operating constraints

#### 3.1 Effects of pressure modulation: simple 1D model

The cathode inlet humidifier was fed with a constant inlet flow rate,  $\dot{q}_{feed}$ , using a mass flow controller (Figure 1, 2), and humidifier air was fed to the fuel cell inlet, with a dry air flow rate  $\dot{q}_{in}$ . Two pressure sensors enable pressure measurement at both fuel cell inlet and outlet. Under back-pressure modulation conditions, pressure variations at fuel cell inlet were observed to differ from pressure variations at fuel cell outlet. More precisely, it appeared that there was a transfer function between  $\tilde{P}_{in}(t)$  and  $\tilde{P}_{out}(t)$ . A simple model has been developed to better understand the transient of pressures in the whole system (Figure 2). From this model, the (dry) air flow rate at the fuel cell inlet is to vary over time from the observations made on pressure. This is due to the significant gas phase volume in the humidifier acting as a reservoir to air, then influencing the air flow rate at its outlet. As a result, it can be deduced that under back-pressure modulation conditions, air flow rate  $\dot{q}_{in}$  at fuel cell inlet is time-dependent, therefore differing from the constant  $\dot{q}_{feed}$ .

Before starting back-pressure modulation, the input pressure and the flow rate at the fuel cell inlet are constant along with the output pressure, so the initial steady-state conditions ( $t \leq 0$ ) are:

Equation 6 
$$P_{out}(t) = \bar{P}_{out}$$

Equation 7 
$$\dot{q}_{in}(t) = \bar{\dot{q}}_{in} = \dot{q}_{feed}$$

Equation 8 
$$P_{in}(t) = \bar{P}_{in} = \bar{P}_{out} + r \cdot \bar{\dot{q}}_{in}$$

where  $r$  (bar.s.NL<sup>-1</sup>) represents the specific pressure drop between inlet and outlet, due to air flowing across the fuel cell. Resistance  $r$  was assumed independent of the gas flow rate. Upon cathode back-pressure modulation, flow rate  $\dot{q}_{feed}$  is constant at any time, and other variables are governed in a first-order approach by (at  $t > 0$ ):

$$\text{Equation 9} \quad P_{out}(t) = \bar{P}_{out} + \Delta P_{out} \cdot \sin(\omega t)$$

$$\text{Equation 10} \quad \dot{q}_{in}(t) = \dot{q}_{feed} - C \left( \frac{dP_{in}(t)}{dt} \right)$$

$$\text{Equation 11} \quad P_{in}(t) = P_{out}(t) + r \cdot \dot{q}_{in}(t)$$

with  $C$  (NL.bar<sup>-1</sup>) is an equivalent capacitor, which represents the gas volume in the humidifier. Fluctuating variables are defined by subtracting their operating steady contribution:  $\tilde{x}(t) = x(t) - \bar{x}$ . Resolution of the previous differential equation system leads to the following harmonic regime:

$$\text{Equation 12} \quad \tilde{P}_{out}(t) = \Delta P_{out} \cdot \sin(\omega t)$$

$$\text{Equation 13} \quad \tilde{q}_{in}(t) = -C\omega |Z_{P-P}(\mathbf{i}, \omega)| \cdot \Delta P_{out} \cdot \cos[\omega t + \phi(Z_{P-P}(\mathbf{i}, \omega))]$$

$$\text{Equation 14} \quad \tilde{P}_{in}(t) = |Z_{P-P}(\mathbf{i}, \omega)| \cdot \Delta P_{out} \cdot \sin[\omega t + \phi(Z_{P-P}(\mathbf{i}, \omega))]$$

where  $Z_{P-P}(\mathbf{i}, \omega)$  is the harmonic pressure-to-pressure impedance, characterized by its modulus and its argument as follows:

$$\text{Equation 15} \quad |Z_{P-P}(\mathbf{i}, \omega)| = \frac{1}{\sqrt{1+(\tau\omega)^2}}$$

$$\text{Equation 16} \quad \phi(Z_{P-P}(\mathbf{i}, \omega)) = -\text{atan}(\tau\omega)$$

$$\text{Equation 17} \quad \tau = r \cdot C$$

The equations above depict that the humidifier volume has a significant role in influencing the flow rate and the pressure at fuel cell inlet. The associated capacitive parameter  $C$  has been assumed to be proportional to the humidifier void (gas) volume  $V_{void}$ , according to

Equation 18 
$$C \approx V_{void} \cdot \left( \frac{V_0}{R \cdot T_{hum}} \right)$$

where  $V_0$  is the normal molar volume (22.4 NL.mol<sup>-1</sup>). Preliminary measurements were carried out to compare this first-order approach with experimental data, at 150 mbar above the atmospheric pressure for  $\bar{P}_{out}$ , 43.1 °C for  $T_{hum}$ , and 0.83 NL.min<sup>-1</sup> for  $\dot{q}_{feed}$  corresponding to the air flow rate supplied for 20 A as fuel cell current and 2.5 as oxygen stoichiometric factor. The pressure drop obtained in steady-state was 12 mbar, yielding the estimate for equivalent resistance  $r$  at 1.417 bar.s.NL<sup>-1</sup>. The value of  $C$  can then be calculated for any gas phase volume using Equation 18. Figure 3a and 3b shows Bode plots of experimental  $Z_{p-p}$  modulus and the phase shift obtained for various humidifier gas volumes. Experimental data are compared to the theoretical data deduced from the first-order model with a good agreement.

It can be observed from Figure 3, that the capacitive effect is not prominent at frequencies below 50 mHz, with inlet and outlet pressures in phase, and with insignificant attenuation of signal. On the other hand, for higher frequencies, because of the volume of the gas phase in the humidifier, the inlet pressure follows only partly the excitation in outlet pressure, resulting in lower pressure modulus (Fig. 3a), and phase shift tending gradually to approximately -90° at the highest frequency (Fig. 3b). Besides, high gas phase volumes are the source of significant inertia in the pressure response  $P_{in}$  which explains that the modulus departs from unity from 10 mHz with  $V_{void} = 1.35$  L, whereas for nearly zero gas phase volumes, the dampening effect of the humidifier is to be virtually nil.

### 3.2 Effect of pressure modulation on gas flow rate

The equations above not only depict the effect of output pressure fluctuations on the inlet pressure and gas flow rate but also give out a vital constraint parameter for pressure fluctuations, i.e.,  $\Delta P_{out}$ . The preliminary experiments brought forward the limitations of the EPIS test bench and the constraints on the amplitude of pressure modulation as explained below. Equation 13 shows that the input flow rate can fall below the air flow rate required for hydrogen oxidation related to generation of current  $J$ , which may starve the fuel cell due to lack of oxidizer: this minimum air flow rate termed as  $\dot{q}_{in}^{min}$  corresponds to a stoichiometry factor of air oxygen equal to unity. The lowest value of the inlet air flow rate represents the lowest transient stoichiometric factor of oxygen, which must not go below 1 and referred to  $\dot{q}_{in}^{min}$ .

With use of eq. (13), simulations have been conducted for the example of  $J = 20$  A, for  $\Delta P_{out} = 10$  mbar, and with  $\lambda_{O_2} = 2.5$  at steady state. The results, in the form of the lowest transient stoichiometric factor  $\lambda_{O_2}(t)$ , are shown in Figure 4 depending on the volume of the gas phase in the humidifier. For very low frequencies, the system has time enough to compensate the capacitive effect of the humidifier, so that the air flow rate fed to the cell varies little. On the contrary, at frequencies larger than 100 mHz, the hydraulic system has less time to react to the pulsation, in particular with large gas volumes in the humidifier (Figure 4): under such gas volume conditions, the air flow rate can go below  $\dot{q}_{in}^{min}$  which has to be avoided. To avoid such degradative operation, pressure fluctuations must be largely reduced for frequencies larger than 100 mHz by decreasing pressure fluctuation amplitude  $\Delta P_{out}$ ; additionally, the gas volume in the humidifier must be kept low.

### 3.3 Operating constraints of EPIS

Apart from the above treated hydraulic issue caused by back-pressure modulations and the risk of transient oxygen starvation at “high” frequencies, suitable operating conditions of the modulation had to be found to fulfill various criteria, which are briefly examined below.

1. The pressure modulation amplitude should be large enough to induce observable electrical signals (at least 2 mV), however allowing linear behavior of the system and harmonic cell voltage response.
2. Very low volumes of the gas atmosphere, expected to be preferable (Fig. 3b), were found to result in the entrainment of water droplets in the humidified air stream which can be detrimental to the cell operation and durability. Therefore, the median gas phase volume (850 mL) value was considered for all the tests shown below.
3. Pressure modulation amplitude must be selected depending on the frequency, as shown above, with far lower amplitude over 100-200 mHz.
4. Tolerance of distortion in pressure and voltage response was set at a maximum of 0.1% and 1%, respectively. The above tolerances were shown to be suitable for harmonic modulations. This is partly in relation to the linearity of the hydraulic-electrochemical system considered for efficient use of Fourier analysis.
5. The system is a closed-circuit; hence pressure modulation amplitude at any time  $t$  must be lower than the pressure difference between inlet and outlet of the cathode side at steady state.  
i.e.  $\Delta P_{out}(t) < (\overline{P}_{in} - \overline{P}_{out})$

Keeping the limitations and constraints of the EPIS test bench, extensive empirical work has been carried out to find the optimal back-pressure amplitude, depending on the conditions of cell operation: in most conditions, whereas pressure fluctuation amplitude in the order of 25 mbar can be used between 1 to 10 mHz, the amplitude had to be set at 2 mbar above 200 mHz.

## 4. Results and discussions

### 4.1 Comparison of EIS and EPIS data

The experiments were conducted with partly humidified air (RH=55%) at various current density levels: obtained EIS and EPIS data were plotted in the form of Bode and Nyquist representation, as exemplified by Figure 5 at  $0.8 \text{ A/cm}^2$ . In both spectroscopies, the potential of the cathode referred to the anode potential is measured, and because of low polarization of the anode in hydrogen fuel cells, the signal is principally that of the cathode. As a result, in steady state, cathode potential increases when cathode outlet pressure increases.

As can be seen in EIS spectra recorded at  $0.8 \text{ A/cm}^2$  for comparison purpose (Fig. 5a and 5b), little information can be extracted in the lower-frequency region below 1 Hz.

As shown in Figure 5c, pressure modulation has a significant effect on the cell voltage in the whole frequency domain (1 mHz to 1 Hz): increasing the frequency results in increased modulus whereas the phase shift decreases from 0 to approx.  $-200^\circ$  at 1 Hz. For frequencies typically below 40 mHz, the larger the outlet pressure, the larger the cathode potential, corresponding to positive value of the real part of  $Z_{U-P}$ . However, for larger frequencies, negative real parts were observed, in accordance with phase shift lower than  $-90^\circ$ . Above 400 mHz, the phase shift is near  $-180^\circ$  indicating that maxima of the outlet backpressure correspond to minima of cell voltage fluctuations. Moreover, the phase shift observed during the experimentation was in agreement with the observed phase shift behavior by Engebretsen et al [18], in the frequency range considered here. It can be observed that EPIS phase shift has a different significance than that of

EIS, in particular because of its strong dependence on cell geometry and location of the pressure modulation source [16–18].

The data produced by EPIS in low-frequency region, although not fully interpreted up to now, appears to be rich information from which deeper insights in fuel cell mass transport phenomena could be obtained. Two cases of mass transport phenomena have been investigated as described below.

#### **4.2 EPIS at different oxygen mole fractions**

Rho et al. [19] suggested in their EIS investigation that the significant control by diffusion of the reacting gas in the inert gas can be specifically examined by comparing the phase shift of the system using air to that with pure oxygen. The experimental analysis was done by comparing the polarization curves and EIS of different systems under constant pressure. To verify if EPIS can be used in detection of diffusion control, experiments were carried out with air, or pure oxygen, or a gas mixture containing 50% or 80% oxygen. The gas flow rate at the inlet of the humidifier were kept unchanged for the four spectra –the oxygen excess varying accordingly -, so that water management conditions in the cell be the same in all cases.

The data example presented were obtained at  $0.2 \text{ A.cm}^{-2}$  at 20% RH, for which no flooding of the cell could occur, as checked by water management investigations (not shown here). As seen in Figure 6, it was observed that both impedance modulus and phase shift exhibit significant changes in the frequency range 10 mHz - 1 Hz: the range was revealed as sufficient because of the limited changes in impedance modulus and phase shift below 10 mHz (data not shown).

The modulus decreases strongly with increasing oxygen mole fraction and is at its lowest (and is constant) with pure oxygen (Fig. 6a). It can be deduced that the smaller the mole fraction of

oxygen in a mixture (below 0.5), the greater the modulus variation, in accordance with Rho et al.'s observations for EIS [19]. Moreover, the most significant differences in the impedance modulus are observed from 300 to 800 mHz which reveals the significant control of gas diffusion in low O<sub>2</sub>-containing gas mixtures. Besides, the phase shift observed with pure oxygen is always larger than -20°, with a very flat minimum near 50 mHz (Fig. 6b), with a striking difference from the phase shift observed with air (Fig. 5c, 6a) or even with 50 % oxygen in the cathode gas.

These observations might suggest the detection of convective and diffusive mass transfer of oxygen to and through the gas diffusion electrode and the high contribution of nitrogen even at moderate contents in mass transport losses, as shown by both modulus and phase shift profiles of EPIS spectra.

### **4.3 Change in humidification**

The effect of this operating parameter has been studied by considering humidification conditions at 20 and 100 % RH in the air stream to the cathode with dry hydrogen at the anode. As confirmed by water management investigations, higher current densities favor the presence of liquid water, with increased water back-diffusion flux: at 0.8 A/cm<sup>2</sup> and for RH=20%, approx. 11% of the water exiting the cell is in liquid state, whereas the fraction attains 49% for 100% RH. Figure 7 shows the two humidification conditions used for EPIS tests for observation of water management issues such as flooding or hydration imbalance. Data are shown in both Bode and Nyquist plots. In figure 7a, the phase shifts tend gradually to -200 ° as the frequency increases but they do not exhibit any noticeable difference for the two humidification conditions. Below 50 mHz, the impedance modules are approximately similar and remain notably constant. At higher frequency, they increase but to a lesser extent at higher humidity: pressure oscillation

appears to affect less the cell voltage in the presence of liquid water in this frequency domain. further investigations should be carried out to better understand the link between water presence and modulus variations for frequency larger than 50 mHz.

## **5. Conclusions**

A test bench for possible experimental validation of EPIS has been successfully designed and set up, and so were the operating conditions for EPIS. Tests have been thoroughly examined for safe operation of the cell and modulation signals far larger than the electrical noise with restricted distortion of the voltage fluctuations. EPIS could then successfully be applied to PEMFC for possible characterization and resolution of various transport phenomena. Simple scenarios like different oxygen mole fraction and varied humidification conditions at the cathode (with the dry anode) have been tested upon application of periodic modulations of the cathode backpressure at constant current density. Oxygen partial pressure and the significance of liquid water in the cell have both affected the modulus of impedance that increased with increasing frequency. This increase is attenuated with increasing oxygen molar fraction and the ratio of liquid water. Except for pure oxygen, the decreasing variations of the phase shift with the frequency, does not shown real differences between all experiments. Moreover, the regular variation of the phase shift with the frequency with diluted-O<sub>2</sub> gases may be used to characterize the gas diffusion to the catalyst layer after development of a suitable modeling tool.

To conclude, whereas EIS is powerful for the detection of charge transfer and ohmic losses, EPIS can be a useful tool to understand, resolve various transport phenomena, while being a complementary diagnosis tool for fuel cell operation and evidence of troublesome situations.

However, as illustrated above, more fundamental work must be carried out for more accurate interpretation of the signals recorded.

### **Acknowledgments**

The authors would like to thank the DFG and ANR-EPISTEL (ANR-17-CE05-0031) for the Ph.D. grant support for A.V. Shirsath and the funding of the overall project.

## List of Abbreviations

$C$	Humidifier volume acting as a capacitor (NL.bar <sup>-1</sup> )
$j$	Current density (A.cm <sup>-2</sup> )
$P$	Relative pressure (bar)
$\bar{P}$	Mean pressure (bar)
$\tilde{P}$	Instantaneous pressure (bar)
$\dot{q}_{feed}$	Constant gas volumetric flow rate fed to humidifier (NL.s <sup>-1</sup> )
$\bar{q}_{in}$	Mean gas volumetric flow rate at fuel cell inlet (NL.s <sup>-1</sup> )
$\tilde{q}_{in}$	Instantaneous gas volumetric flow rate at fuel cell inlet (NL.s <sup>-1</sup> )
$q_{in}^{min}$	Minimum inlet gas flow rate required for reliable operation of fuel cell (NL.s <sup>-1</sup> )
$r$	Pressure drop across fuel cell due to air flow (bar.s.NL <sup>-1</sup> )
$R$	Universal gas constant (J.mol <sup>-1</sup> .K <sup>-1</sup> )
$t$	Time (s)
$T$	Temperature (°C)
$\tilde{U}$	Instantaneous cell voltage (V)
$V_0$	Normal molar volume (NL)
$V_{void}$	Gas phase (void) volume inside humidifier (NL)
$Z$	Impedance (dimensionless <u>or</u> mΩ <u>or</u> μV.Pa <sup>-1</sup> )

## Subscripts

in	Inlet
----	-------

out	Outlet
H <sub>2</sub>	Hydrogen
O <sub>2</sub>	Oxygen
P-P	Pressure-pressure
U-J	Voltage-current
U-P	Voltage-pressure

**Greek symbols**

$\Delta P_{out}$	Pressure modulation amplitude (bar)
$\phi$	Pressure-pressure phase shift (°)
$\omega$	Angular frequency (rad.s <sup>-1</sup> )
$\tau$	Characteristic time constant = r.C (s)
$\lambda$	Stoichiometric factor
$\phi$	Voltage-pressure phase shift (°)

## References

- [1] IPCC, Summary for Policymakers. Global Warming of 1.5°C., in: Glob. Warm. 1.5°C. An IPCC Spec. Rep. Impacts Glob. Warm. 1.5°C above Pre-Industrial Levels Relat. Glob. Greenh. Gas Emiss. Pathways, Context Strength. Glob. Response to Threat Clim. Chang., 2018. doi:10.1017/CBO9781107415324.
- [2] James Larminie, Fuel Cell Systems Explained, John Wiley Sons Ltd, Atrium, South. Gate, Chichester, West Sussex PO19 8SQ, Engl. (2003) 406.  
[http://cs5450.userapi.com/u11728334/docs/765b149a3617/4857X\\_02.pdf](http://cs5450.userapi.com/u11728334/docs/765b149a3617/4857X_02.pdf) (accessed June 20, 2018).
- [3] R.P. O'Hayre, S.-W. Cha, C.W. G., P.F. B., Fuel Cell Fundamentals, 2nd Ed., John Wiley Sons. (2009).
- [4] D. Arora, C. Bonnet, M. Mukherjee, S. Raël, F. Lapique, Direct hybridization of PEMFC and supercapacitors: Effect of excess hydrogen on a single cell fuel cell durability and its feasibility on fuel cell stack, *Electrochim. Acta.* 310 (2019) 213–220.  
doi:10.1016/j.electacta.2019.04.073.
- [5] D. Arora, C. Bonnet, M. Mukherjee, S. Arunthanayothin, A. Shirsath, M. Lundgren, M. Burkardt, S. Kmiotek, S. Raël, F. Lapique, S. Guichard, Long term study of directly hybridized proton exchange membrane fuel cell and supercapacitors for transport applications with lower hydrogen losses, *J. Energy Storage.* (2020). doi:10.1016/j.est.2020.101205.
- [6] F. Lapique, M. Belhadj, C. Bonnet, J. Pauchet, Y. Thomas, A critical review on gas diffusion micro and macroporous layers degradations for improved membrane fuel cell durability, *J. Power Sources.* (2016). doi:10.1016/j.jpowsour.2016.10.037.
- [7] H.H. Wang, X.-Z. Yuan, H. Li, PEM fuel cell durability handbook. PEM fuel cell diagnostic tools, CRC Press/Taylor & Francis, 2012.
- [8] M.E. Orazem, B. Tribollet, *Electrochemical Impedance Spectroscopy*, John Wiley & Sons, Inc., Hoboken, NJ, USA, 2008. doi:10.1002/9780470381588.
- [9] J. Wu, X.Z. Yuan, H. Wang, M. Blanco, J.J. Martin, J. Zhang, Diagnostic tools in PEM fuel cell research: Part I Electrochemical techniques, *Int. J. Hydrogen Energy.* 33 (2008) 1735–1746. doi:10.1016/j.ijhydene.2008.01.013.
- [10] M. Amirinejad, S. Rowshanzamir, M.H. Eikani, Effects of operating parameters on performance of a proton exchange membrane fuel cell, *J. Power Sources.* 161 (2006) 872–875.  
doi:10.1016/j.jpowsour.2006.04.144.
- [11] J. Zhang, C. Song, J. Zhang, R. Baker, L. Zhang, Understanding the effects of backpressure on PEM fuel cell reactions and performance, *J. Electroanal. Chem.* 688 (2013) 130–136. doi:10.1016/j.jelechem.2012.09.033.

- [12] A.V. Shirsath, S. Raël, C. Bonnet, L. Schiffer, W. Bessler, F. Lopicque, Electrochemical pressure impedance spectroscopy for investigation of mass transfer in polymer electrolyte membrane fuel cells, *Curr. Opin. Electrochem.* (2020). doi:10.1016/j.coelec.2020.04.017.
- [13] T. V. Reshetenko, G. Bender, K. Bethune, R. Rocheleau, Systematic study of back pressure and anode stoichiometry effects on spatial PEMFC performance distribution, *Electrochim. Acta.* 56 (2011) 8700–8710. doi:10.1016/j.electacta.2011.07.058.
- [14] B. Zhou, W. Huang, Y. Zong, A. Sobiesiak, Water and pressure effects on a single PEM fuel cell, *J. Power Sources.* 155 (2006) 190–202. doi:10.1016/j.jpowsour.2005.04.027.
- [15] A.M. Niroumand, W. Mérida, M. Eikerling, M. Saif, Pressure-voltage oscillations as a diagnostic tool for PEFC cathodes, *Electrochem. Commun.* 12 (2010) 122–124. doi:10.1016/j.elecom.2009.11.003.
- [16] P. Hartmann, D. Grübl, H. Sommer, J. Janek, W.G. Bessler, P. Adelhelm, Pressure Dynamics in Metal – Oxygen (Metal – Air) Batteries: A Case Study on Sodium Superoxide Cells, *J. Phys. Chem. C.* 2 (2014) 1461–1471. doi:10.1021/jp4099478.
- [17] D. Grübl, J. Janek, W.G. Bessler, Electrochemical Pressure Impedance Spectroscopy (EPIS) as Diagnostic Method for Electrochemical Cells with Gaseous Reactants: A Model-Based Analysis, *J. Electrochem. Soc.* 163 (2016) A599–A610. doi:10.1149/2.1041603jes.
- [18] E. Engebretsen, T.J. Mason, P.R. Shearing, G. Hinds, D.J.L. Brett, Electrochemical pressure impedance spectroscopy applied to the study of polymer electrolyte fuel cells, *Electrochem. Commun.* 75 (2017) 60–63. doi:10.1016/j.elecom.2016.12.014.
- [19] Y.W. Rho, Mass Transport Phenomena in Proton Exchange Membrane Fuel Cells Using O<sub>2</sub>/He, O<sub>2</sub>/Ar, and O<sub>2</sub>/N<sub>2</sub> Mixtures, *J. Electrochem. Soc.* 141 (1994) 2084. doi:10.1149/1.2055065.

## Figure Captions

Fig. 1 Experimental bench with a 100 cm<sup>2</sup> PEM fuel cell for EPIS measurements

Figure 2. Cathode side-feed line, with on the right side the equivalent circuit model

Figure 3 Influence of gas phase volume of humidifier on (a): ratio of inlet pressure ( $\tilde{P}_{in}$ ) and outlet pressure ( $\tilde{P}_{out}$ ) (b): on the phase shift between inlet and outlet pressure

Figure 4: Influence of gas phase volume in the humidifier on the ratio of the lowest  $\dot{q}_{in}$  value over the minimum air flow rate ( $\lambda_{O_2}=1$ ) (calculated data only)

Figure 5. Representation of EIS measurements: (a) Bode plot, (b) Nyquist plot, and EPIS measurements (c) Bode plot, (d) Nyquist plot. The fuel cell was operated at  $j = 0.8 \text{ A/cm}^2$ , 55 °C, RH=55% at the cathode and dry gas to the anode. Solids lines are only for illustration.

Figure 6: Comparison of (a) impedance modulus and phase shift (b) at different oxygen mole fraction with the same operating conditions;  $j=0.2 \text{ A/cm}^2$ , RH=20%

Figure 7: Comparison of EPIS measurements: (a) Bode plot, and (b) Nyquist plot at different humidification conditions at  $0.8 \text{ A.cm}^{-2}$ . Solids lines are only for illustration.

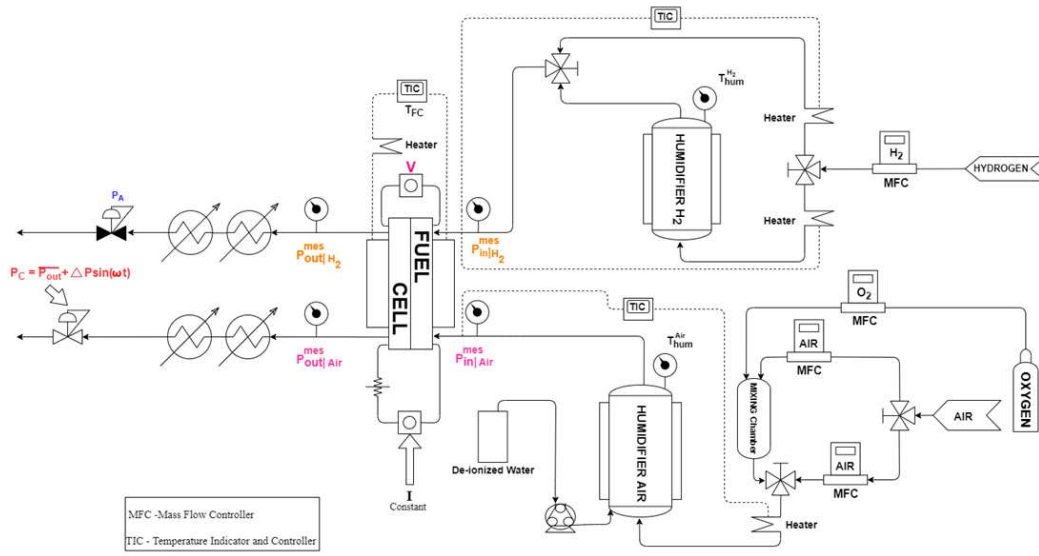


Fig. 1 Experimental bench with a 100 cm<sup>2</sup> PEM fuel cell for EPIS measurements

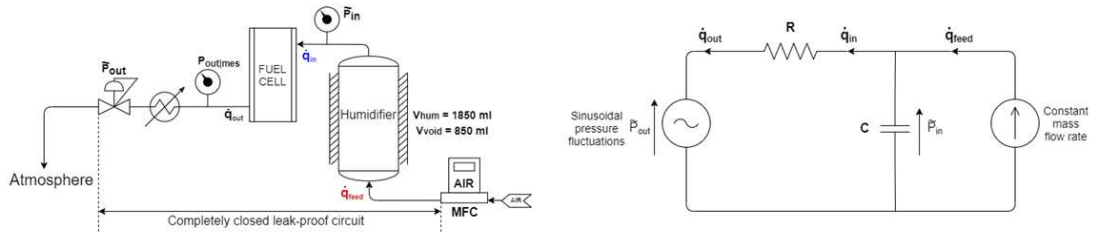
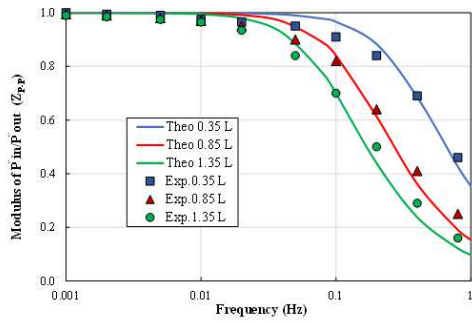
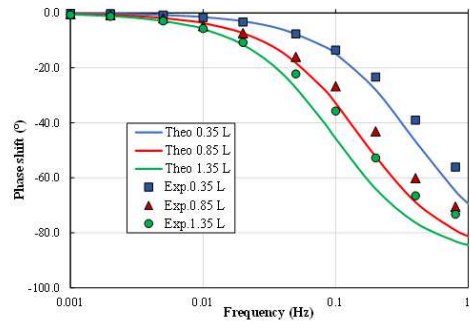


Figure 2. Cathode side-feed line, with on the right side the equivalent circuit model



(a)



(b)

Figure 3 Influence of void volume of humidifier on (a): ratio of inlet pressure ( $\tilde{P}_{in}$ ) and outlet pressure ( $\tilde{P}_{out}$ ) (b):  
on the phase shift between inlet and outlet pressure

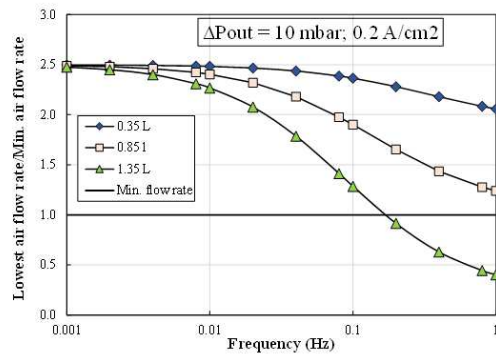


Figure 4 Influence of void volume of humidifier on the ratio of the lowest  $\dot{q}_{in}$  value over the minimum air flow rate ( $\lambda_{O_2}=1$ ) (calculated data only)

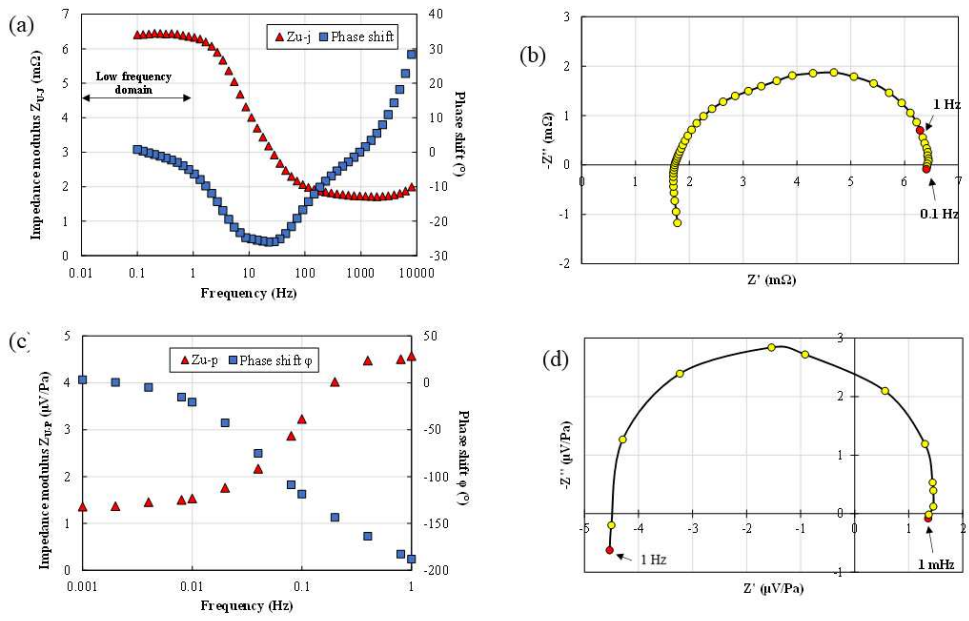


Figure 5.

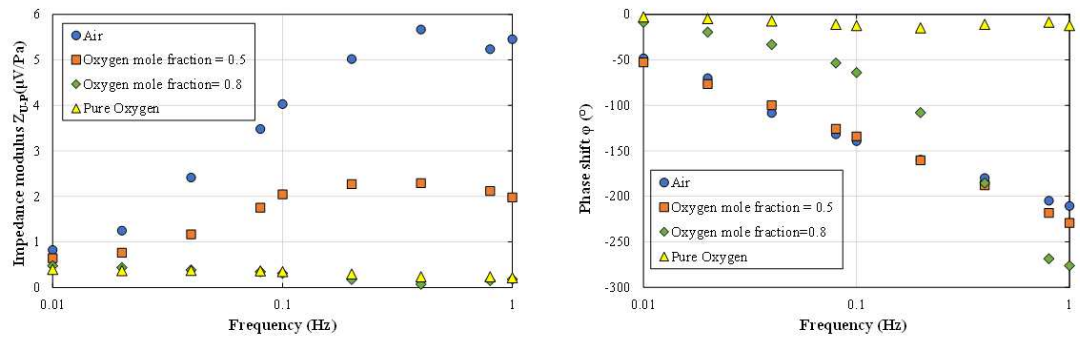


Figure 6: Comparison of (a) impedance modulus and phase shift (b) at different oxygen mole fraction with the same operating conditions;  $j=0.2 \text{ A/cm}^2$ ,  $\text{RH}=20\%$

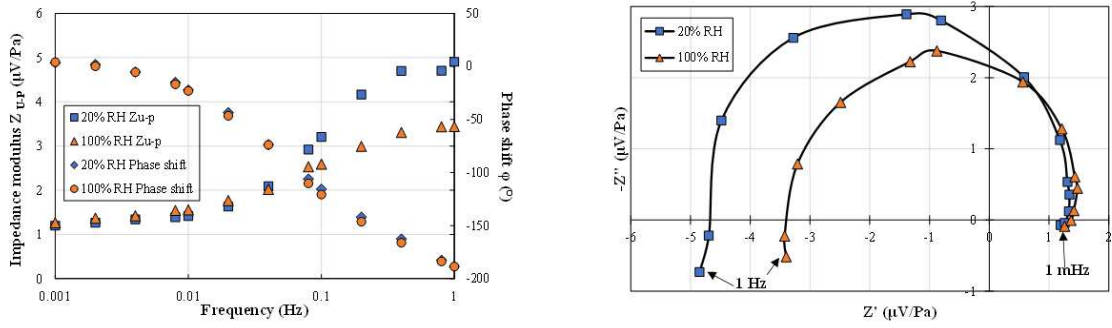


Figure 7: Comparison of EPIS measurements: (a) Bode plot, and (b) Nyquist plot at different humidification conditions at 0.8 A.cm<sup>-2</sup>. (Solids lines are only for illustration)